High energy emission from massive star clusters

A.M. Bykov
High Energy Astrophysics
Ioffe Institute, St.Petersburg, Russian Federation

Collaborators: D.C.Ellison, P.E.Gladilin, S.M.Osipov

NGC 253 starburst ROSAT & XMM-Newton

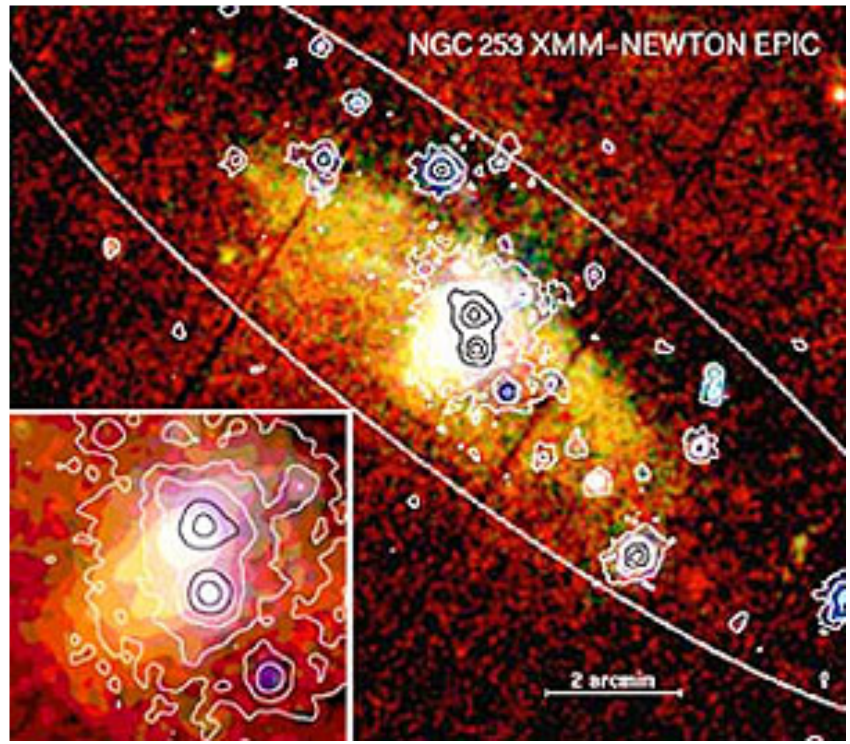

NGC 253 starburst

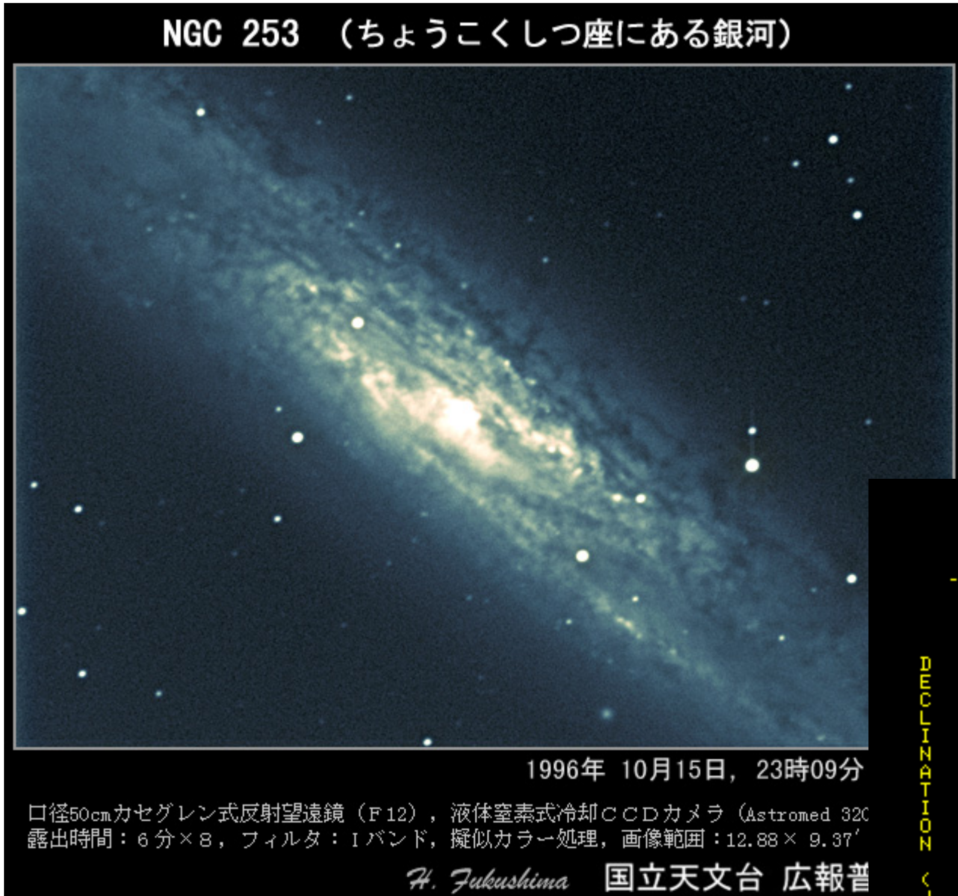

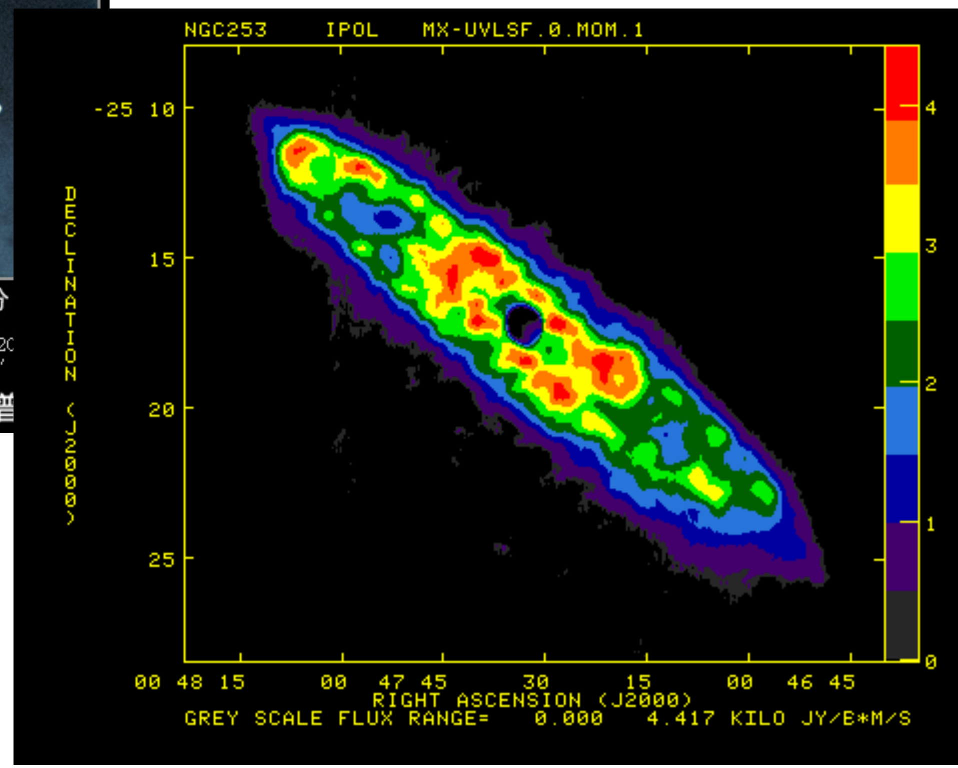

http://www.atnf.csiro.au

SED starburst

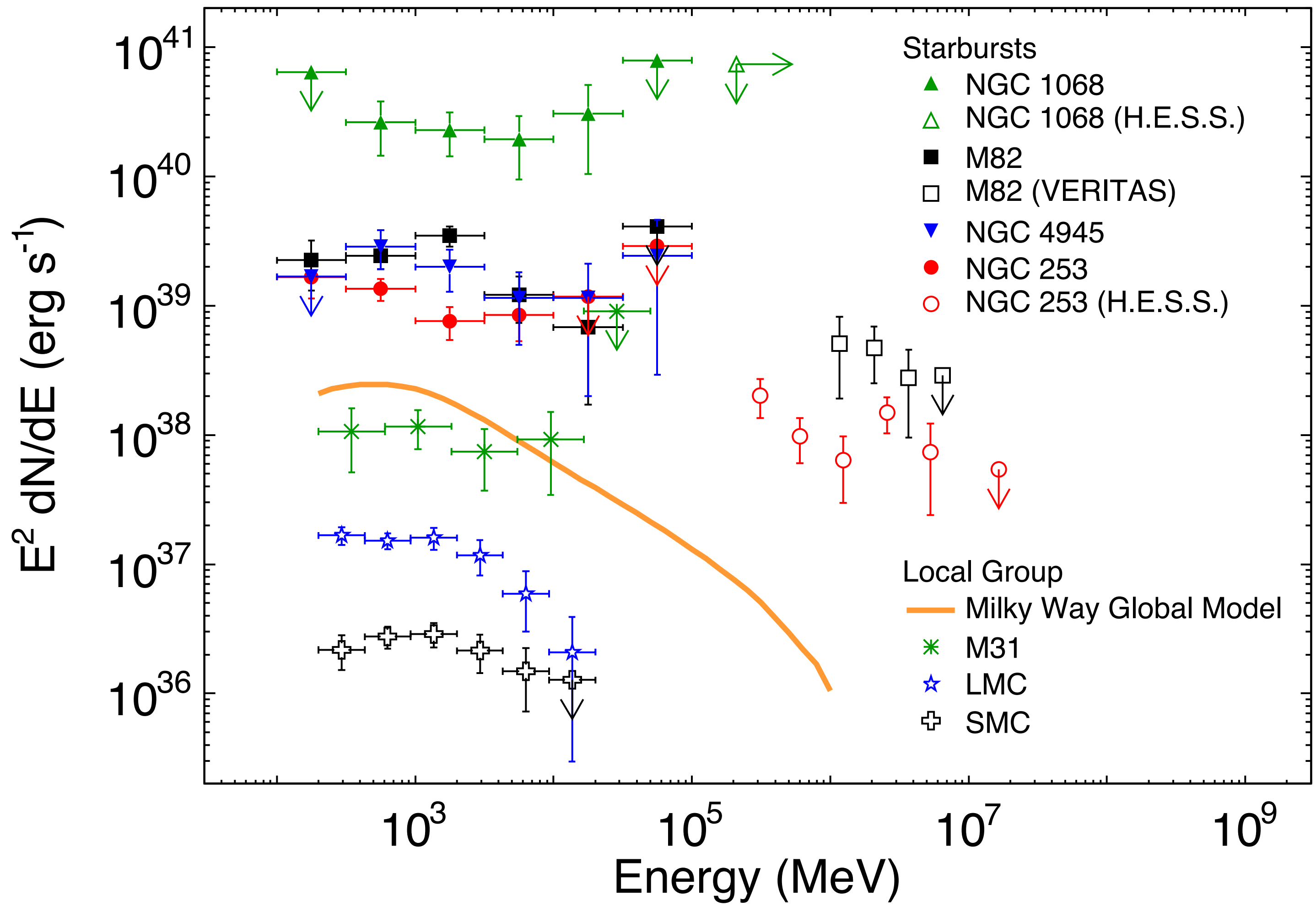

Ackermann + 12

Fermi 30 Dor spectra model

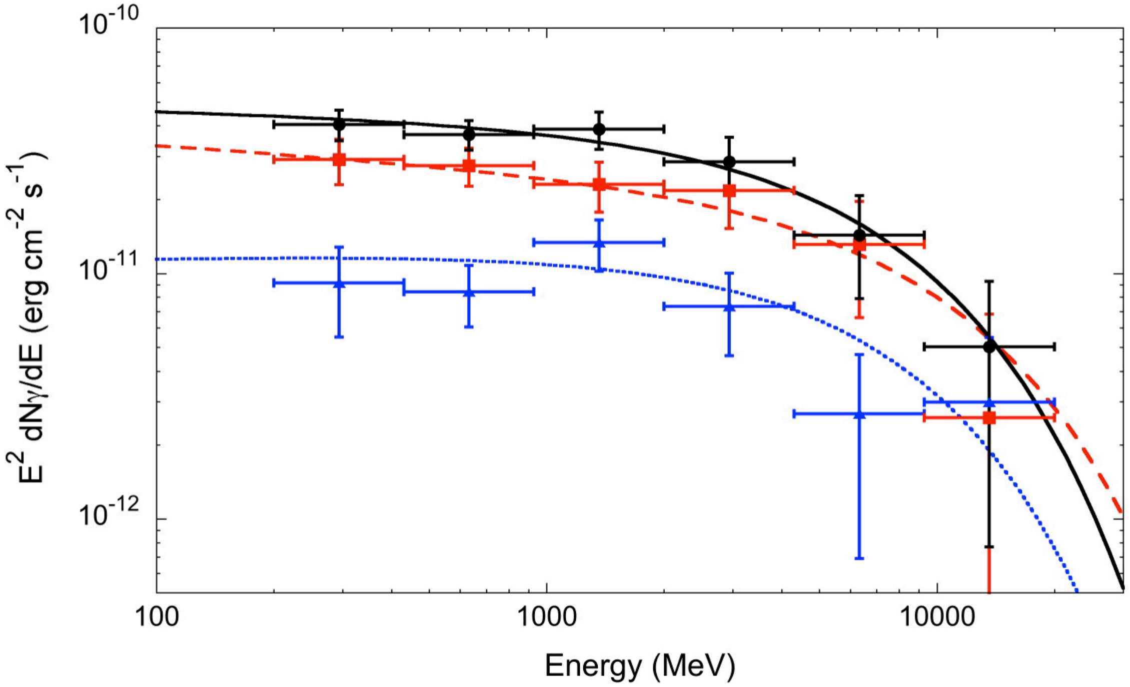

The spiral galaxy NGC 253 is the closest starburst galaxies at 2.6–3.9 Mpc

The starburst nucleus region is a cylinder of $R \approx 150$ pc with the height $H \approx 60$ pc perpendicular to the disk of NGC 253 and symmetric to its mid-plane

The estimated SN rate is about 0.08 yr(-1) in NGC 253, with 0.03 yr(−1) in the starburst region.

The SFR is about 5 $M_\odot$ /yr in the starburst nucleus, which is 0.7 of the whole SFR of NGC 253.

e.g. Abramowski Acero Aharonian + 12

What kind of sources one could expect in starburst?

“Dim” young and “bright” old SNRs?

Hadronic gamma-ray emission from individual young “molecular” SNRs

Fermi images of young SNRs

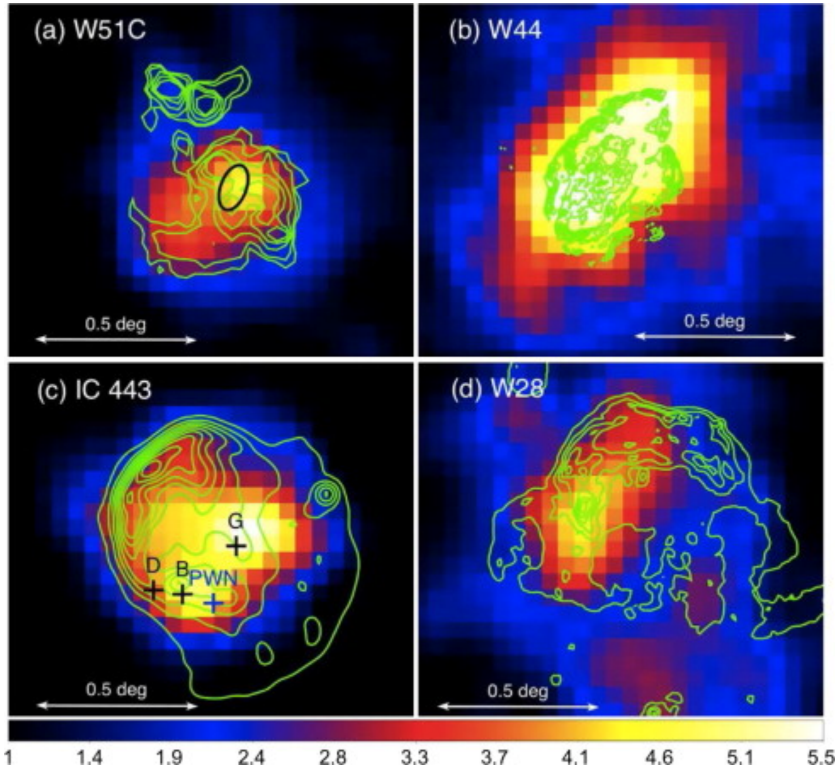

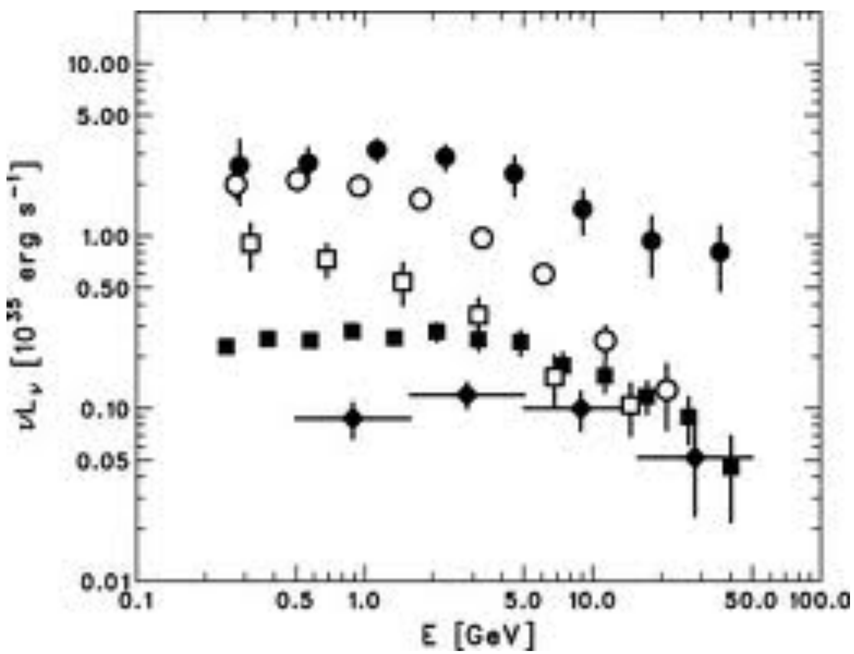

$$L_\gamma \sim 10^{34} - 10^{36} erg / s$$

W51C (filled circles) W44 (open circles);
IC 443 (filled rectangles); W28 (open rectangles)
Cassiopeia A (filled diamonds).

Thompson Baldini Uchiyama 2012

What else one could expect in starburst?

Hadronic gamma-ray emission from superbubbles?

The Carina Nebula (2.3 x 2.3 deg) by ESA's Herschel space observatory

ESA/PACS/SPIRE/T. Preibisch

SB around NGC 1929 in LMC VLT image

ESA/VLT Mejias

Cygnus-X region

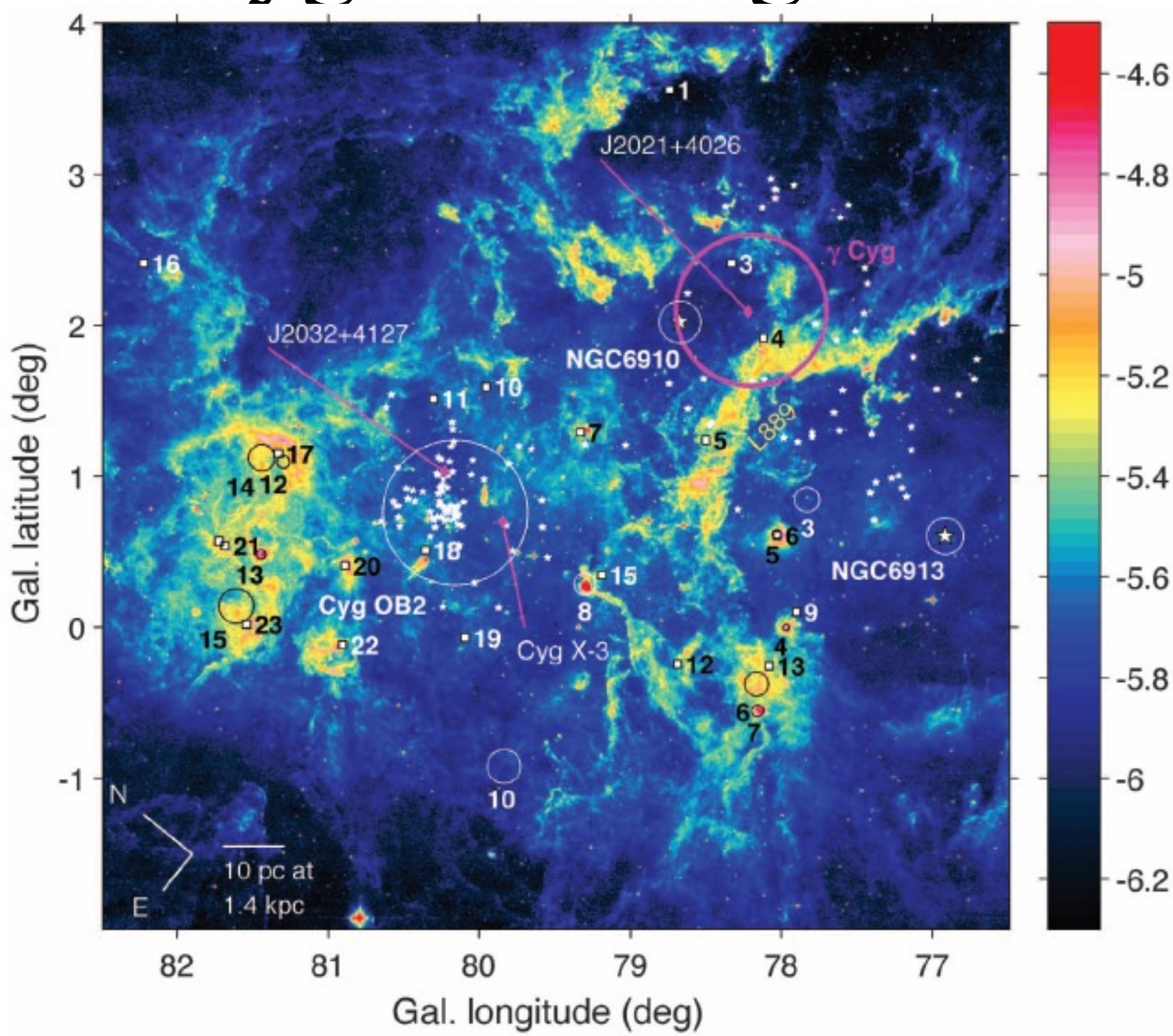

Fig. 1. An 8-μm intensity map of the Cygnus X region from MSX (W m^{-2} sr^{-1}, in log scale), outlining the PDRs. Objects are noted with their names or numbers: Cyg X-3 and pulsars J2021+4026 and J2032+4127 (magenta diamonds); the γ Cygni supernova remnant (magenta circle); OB associations [white or black circles (*7*)]; HII regions [white squares (*10*)]; and OB stars from Cyg OB2 and Cyg OB9 [white stars (*8*, *29*)].

Ackermann + Science 2011

Fermi image of Cygnus superbubble

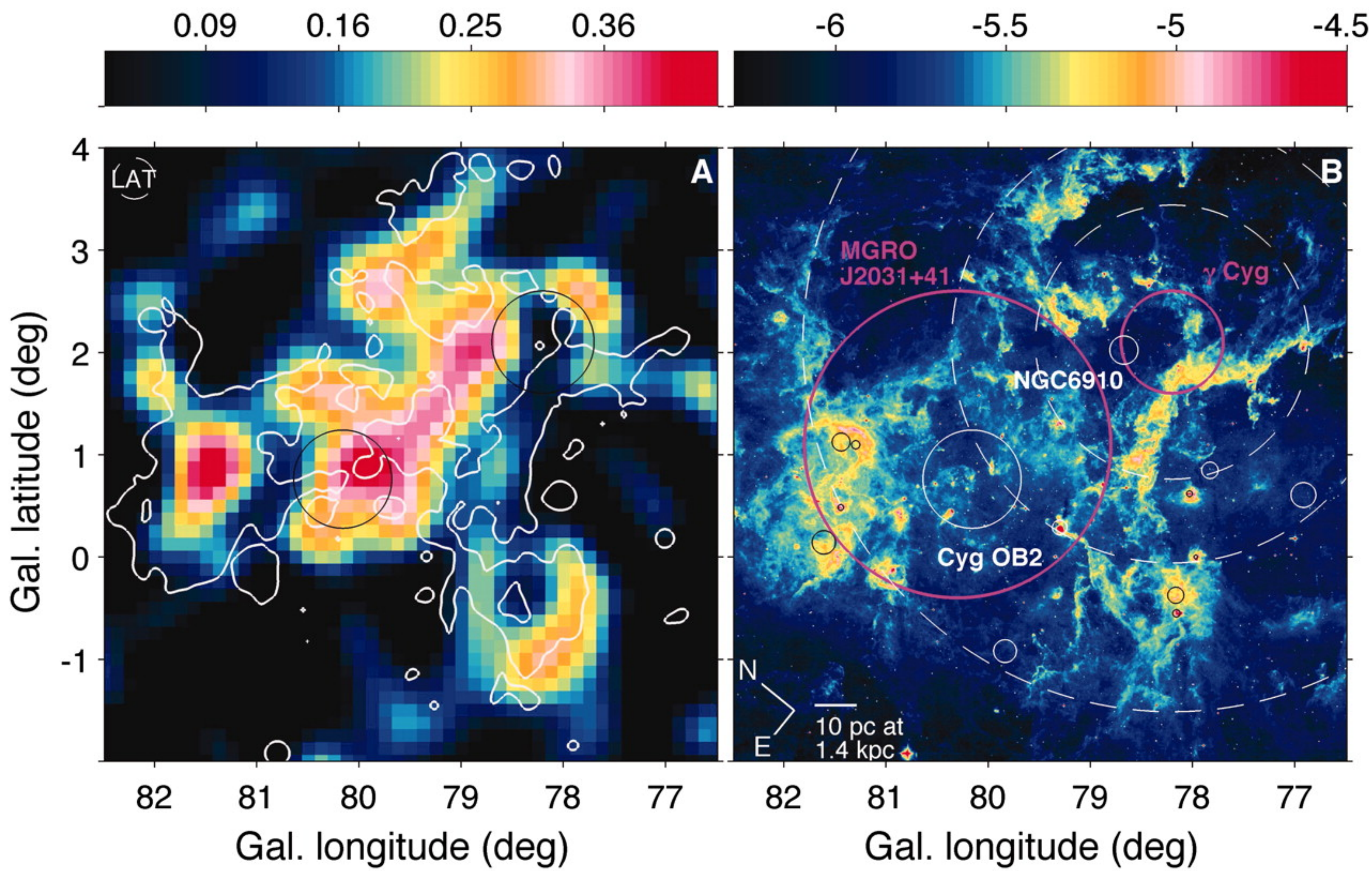

Ackermann + 2011

Fermi image of Cygnus superbubble

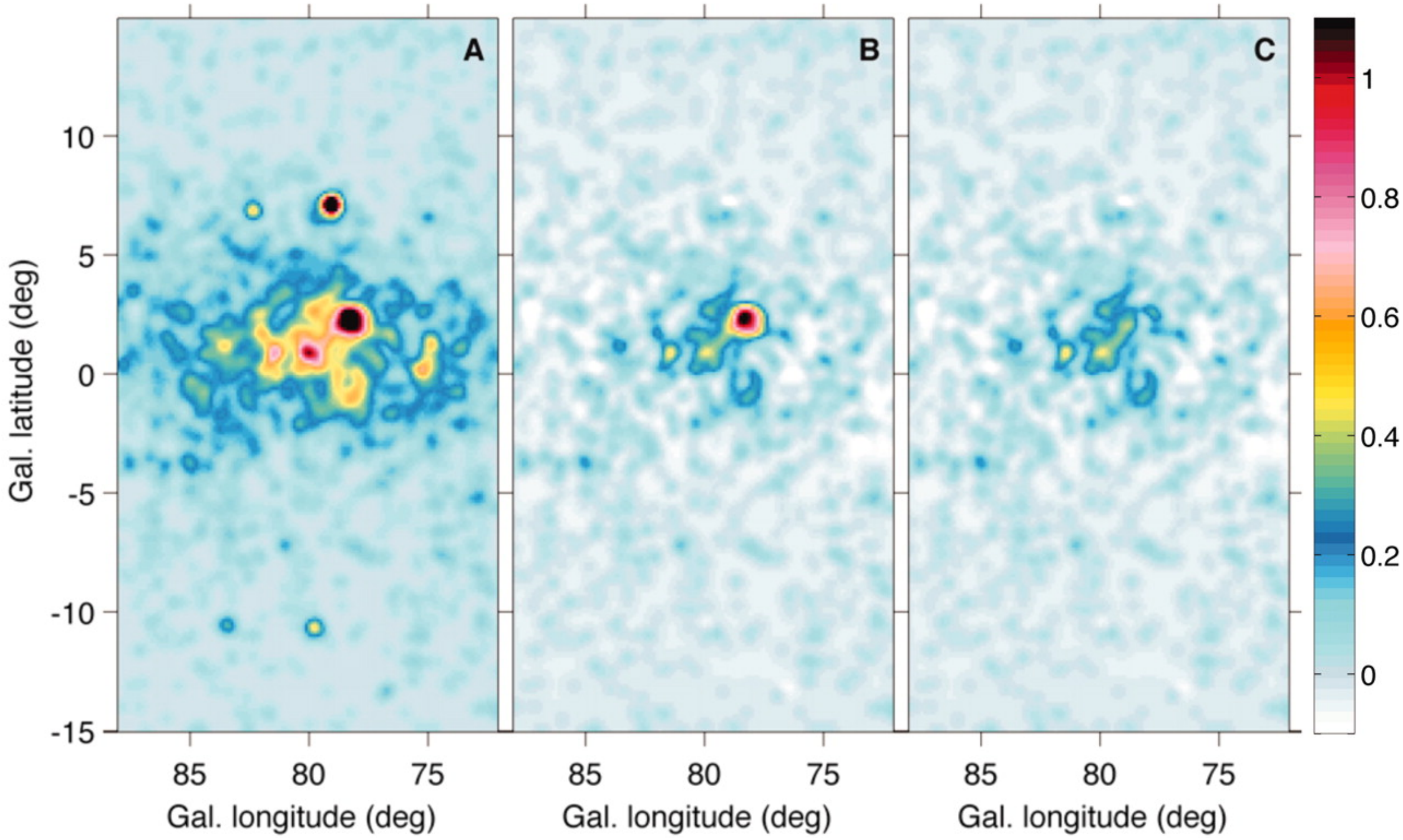

Fig. 2. Photon count maps in the 10- to 100-GeV band (*30*), smoothed with a $\sigma = 0.25°$ Gaussian kernel, obtained for the total emission (**A**), after subtraction of the interstellar background and all known sources but γ Cygni (**B**), and after further removal of the extended emission from γ Cygni (**C**).

Ackermann + Science 2011

The Fermi source is extended of about 50 pc scale size and anti-correlate with MSX

Cygnus X is about 1.5 kpc away. Contain a number of young star clusters and several OB associations. Cygnus OB2 association contains 65 O stars and more than 500 B stars. There is a young supernova remnant Gamma-Cygni and a few gamma-pulsars.

Fermi spectrum of Cygnus superbubble

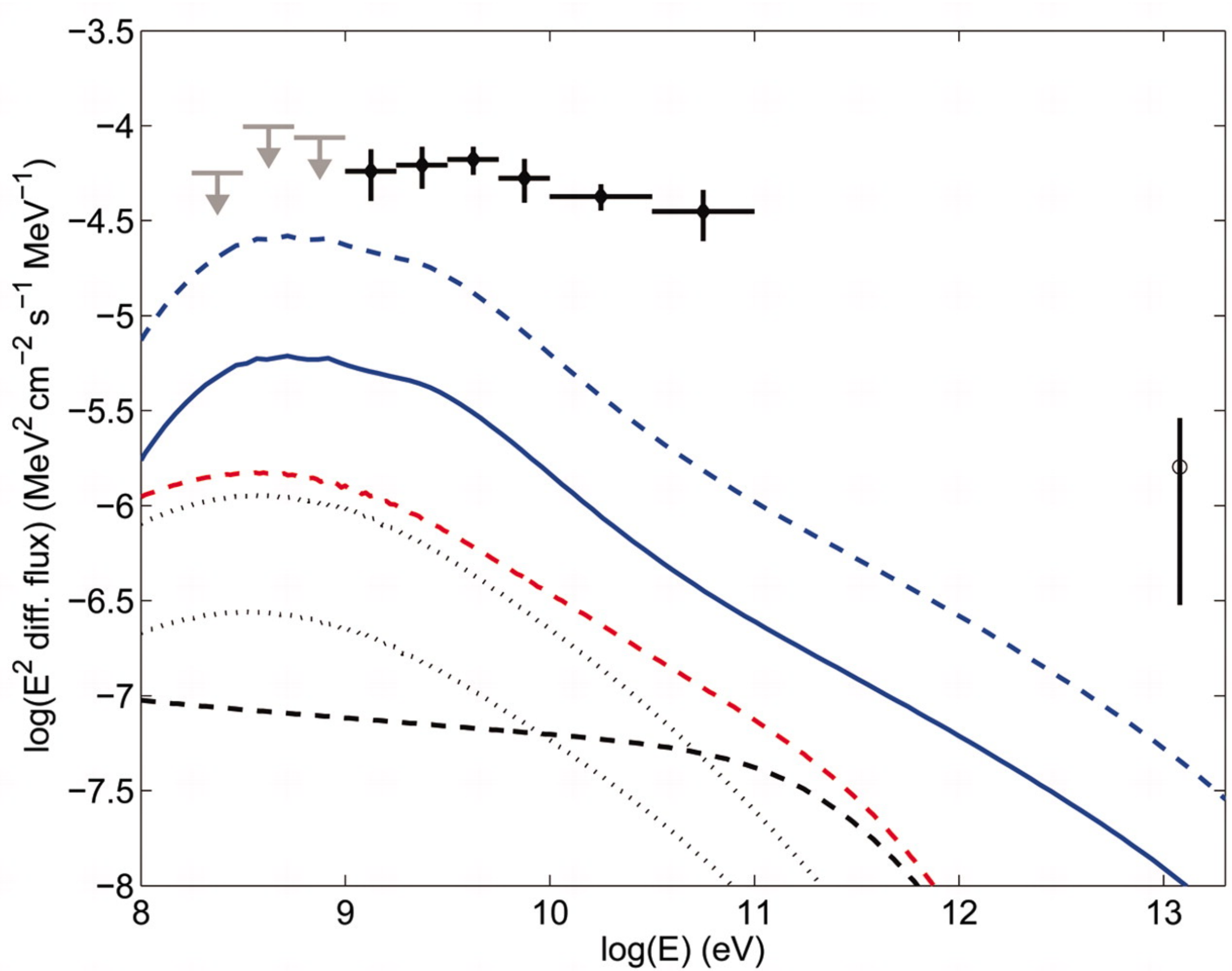

Ackermann + 2011

Simulations with our non-linear kinetic model of relativistic particle acceleration accounting for particle acceleration by multiple shocks and long-wavelength strong turbulence predicted temporal evolution of spectrum

MHD Shock-Turbulence Power Conversion to CRs

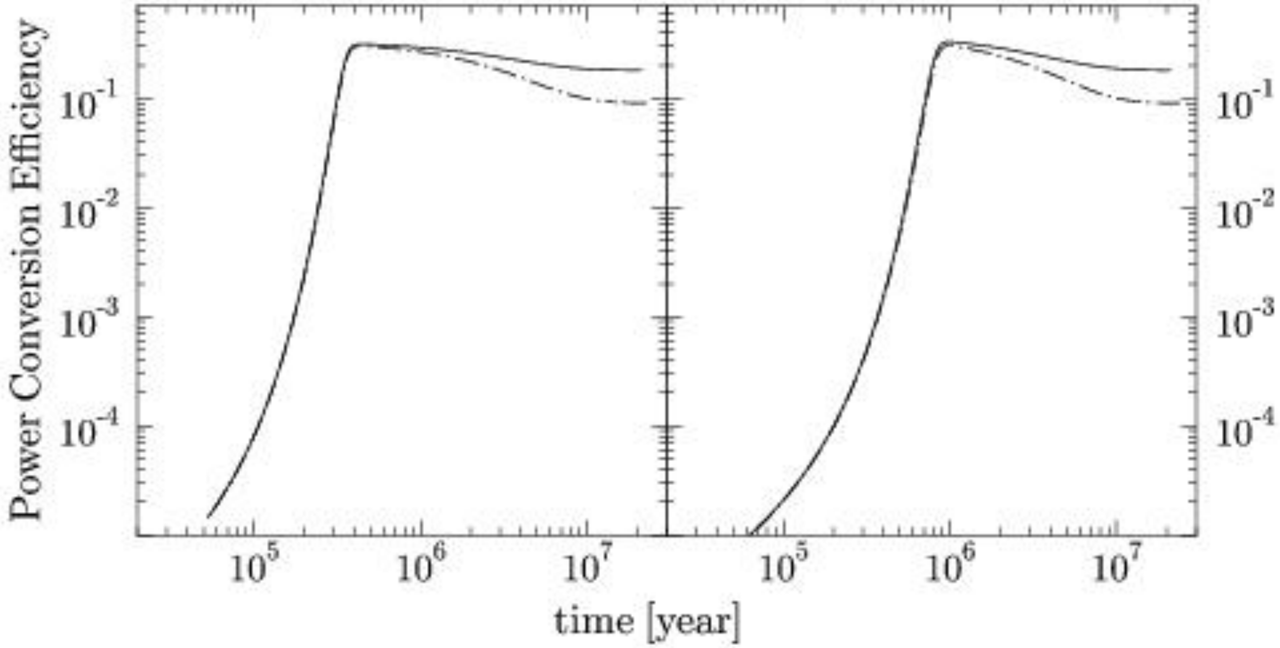

Temporal Evolution of Particle Spectrum

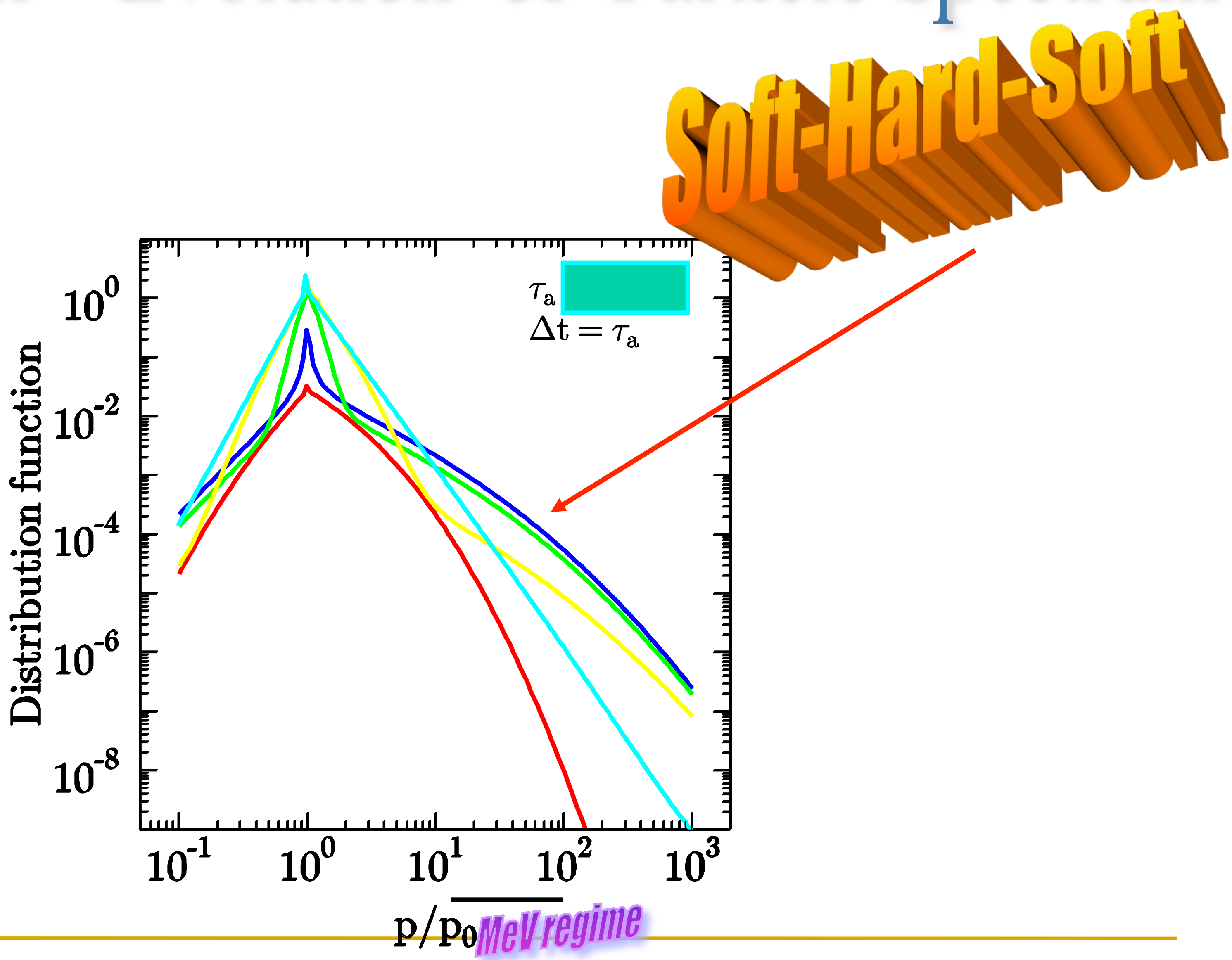

AB Space Sci. Rev. v.99, 317 see also Ferrand & Marcowith

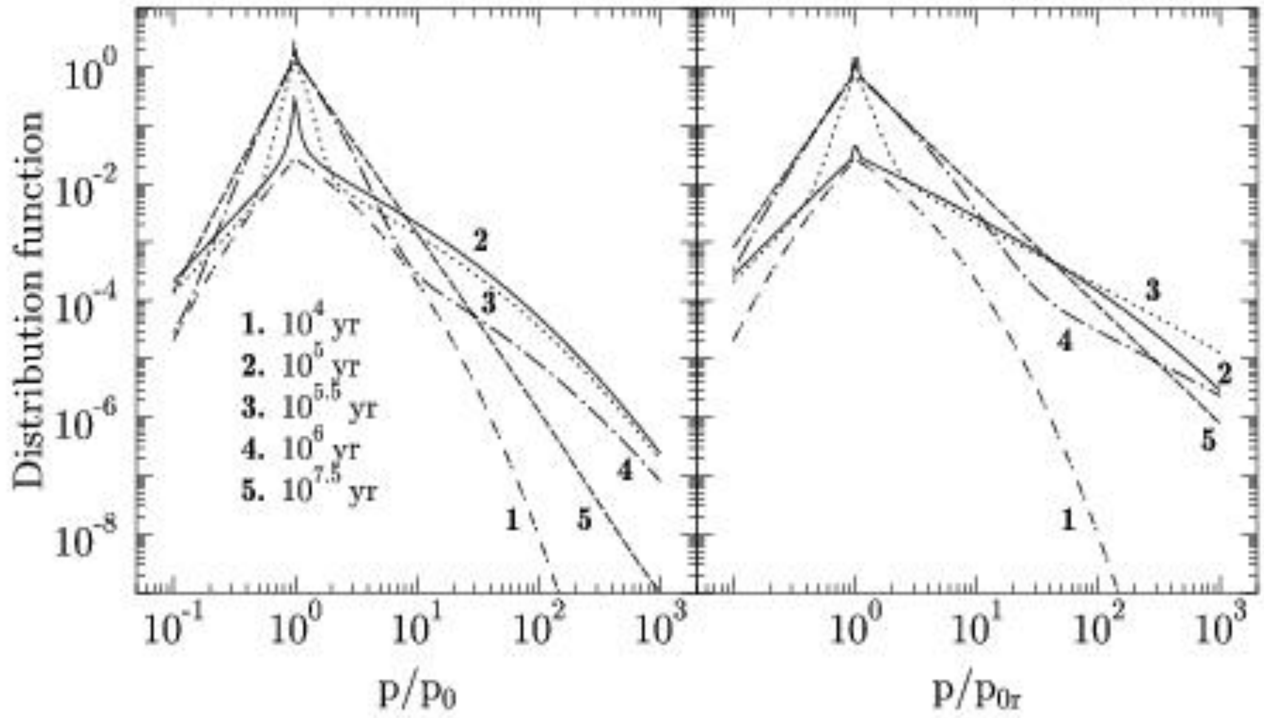

Space Sci. Rev. v.99, 317

Fermi spectrum of Cygnus superbubble can be explained as hadronic emission

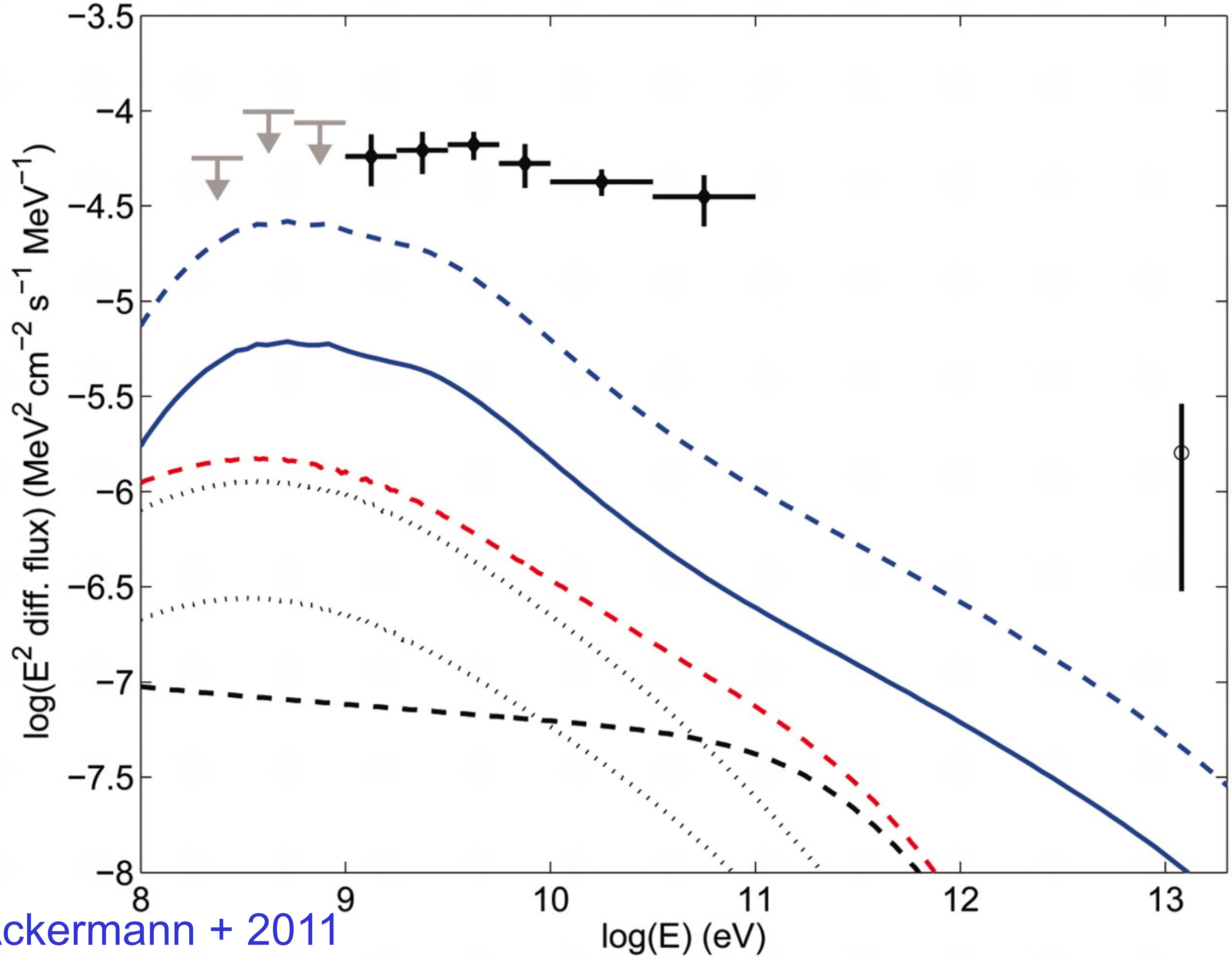

Ackermann + 2011

What else one could expect in starburst?

Hadronic gamma-ray emission from SNR-wind collisions in massive star clusters…

The Progenitor to the Pulsar had an Initial Mass of >40 M_{sun}

- Westerlund 1 contains O6V and O7V stars with initial masses of 35-37 M_{sun} (Clark et al., 2010).
- Its age is <5 Myr.
- At this age, only stars more massive than 40 M_{sun} would have undergone supernovae.

- (from M.Muno)

Westerlund 1

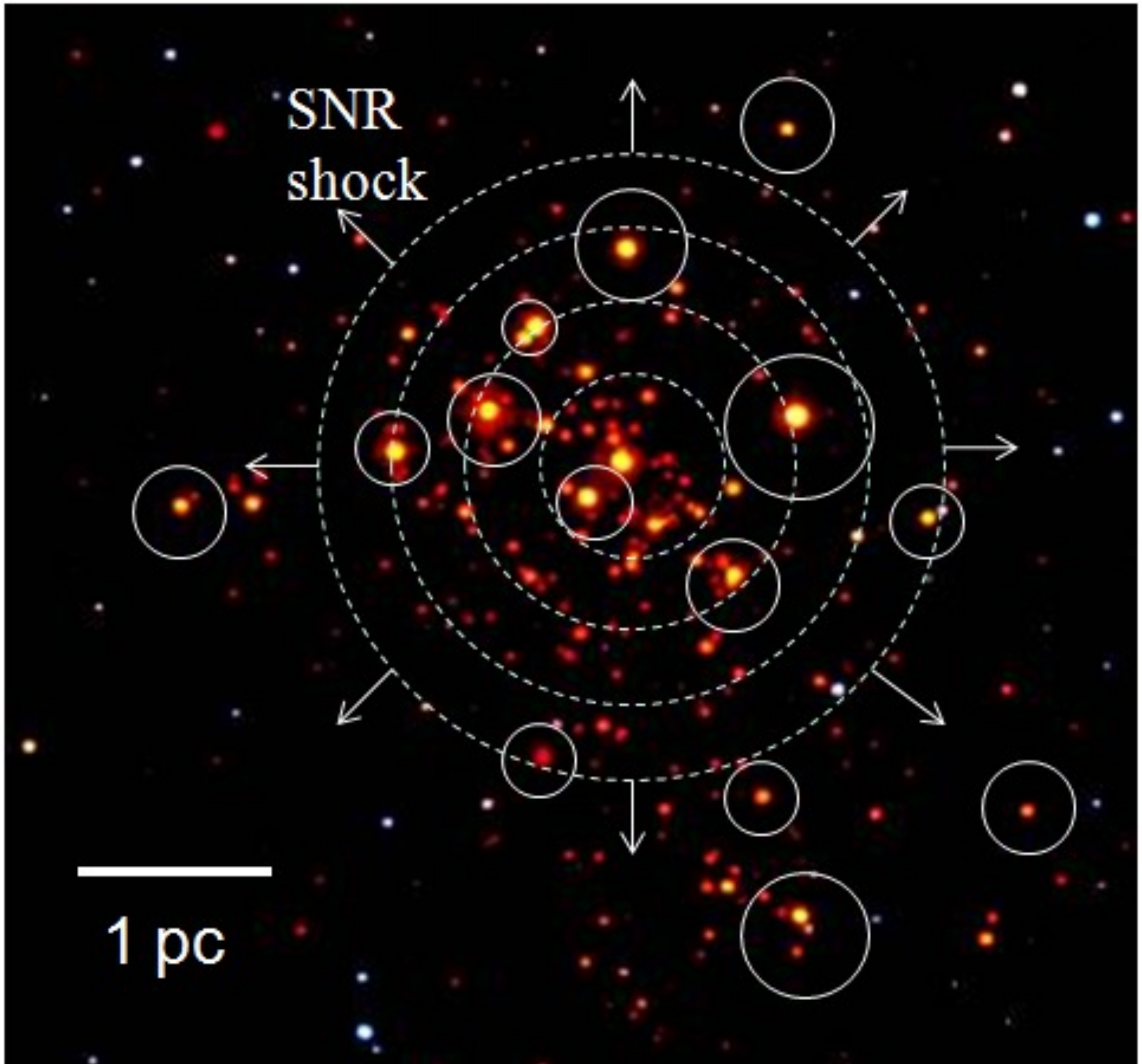

Clark+ 11

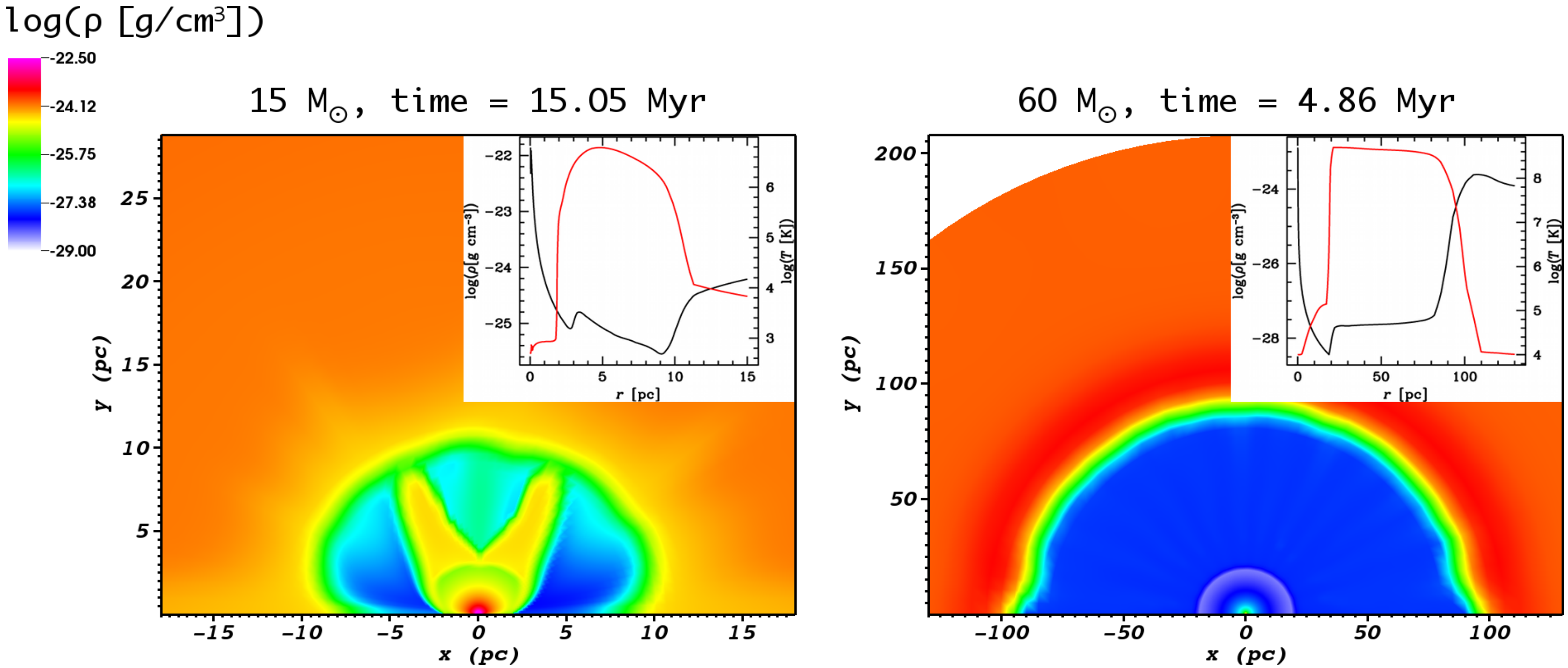

Fig. 4. Typical pre-SN aspect of the CSM around a 15 $M_\odot$ star *(left panel)* ending its stellar life as an RSG (and exploding as a type IIP SN), and around a 60 $M_\odot$ star *(right panel)*, ending as a WR star (exploding as a type Ibc SN). In each panel, we also show the mean density and temperature in the small window as a function of the radius.

Cyril Georgy + A&A v559, A69, 2013

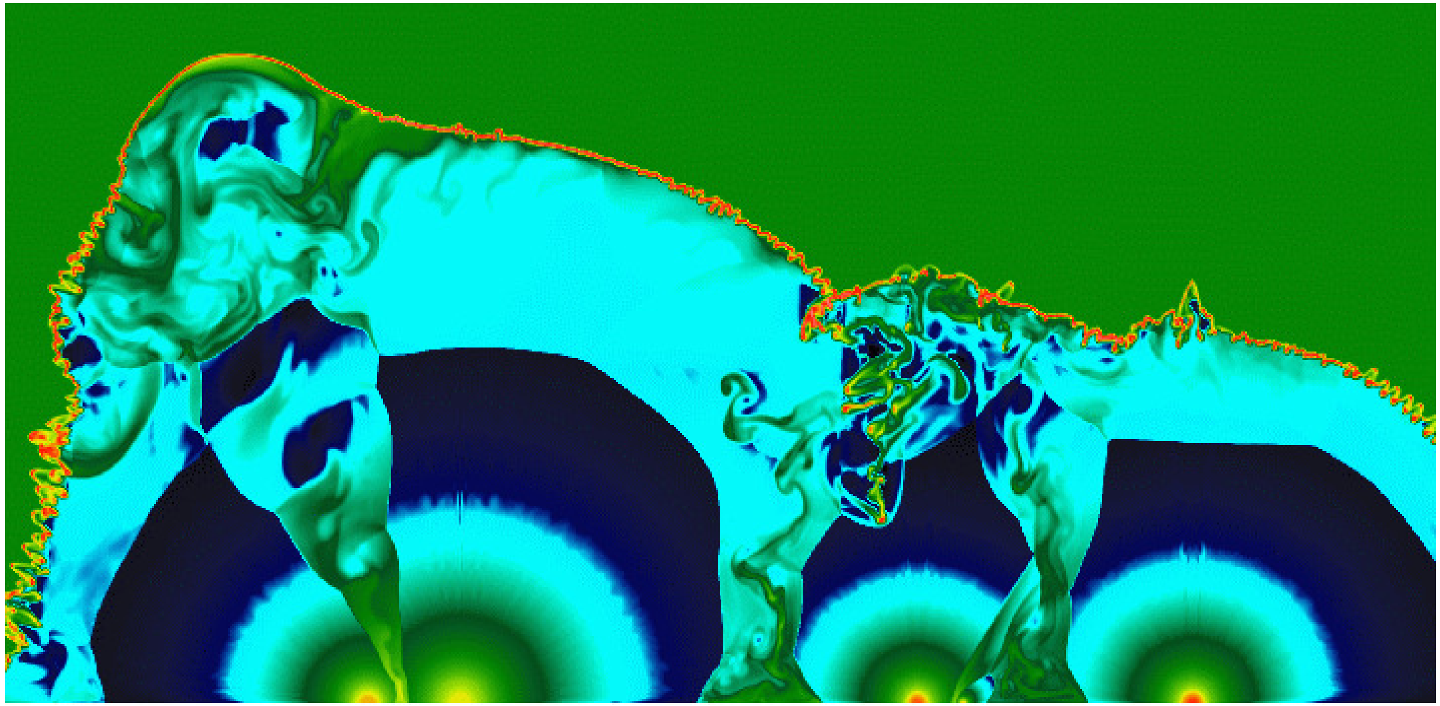

Fig. 14. Axisymmetric simulation of a mini-star cluster of 5 stars shown in density (blue: $0.01/cm^3$, green $1/cm^3$, red $10/cm^3$, white $1000/cm^3$). Thin shell instabilities develop in regions of interactions of different winds and of wind-interstellar medium.

Cyril Georgy + A&A v559, A69, 2013

MASSIVE STAR BINARY SYSTEMS

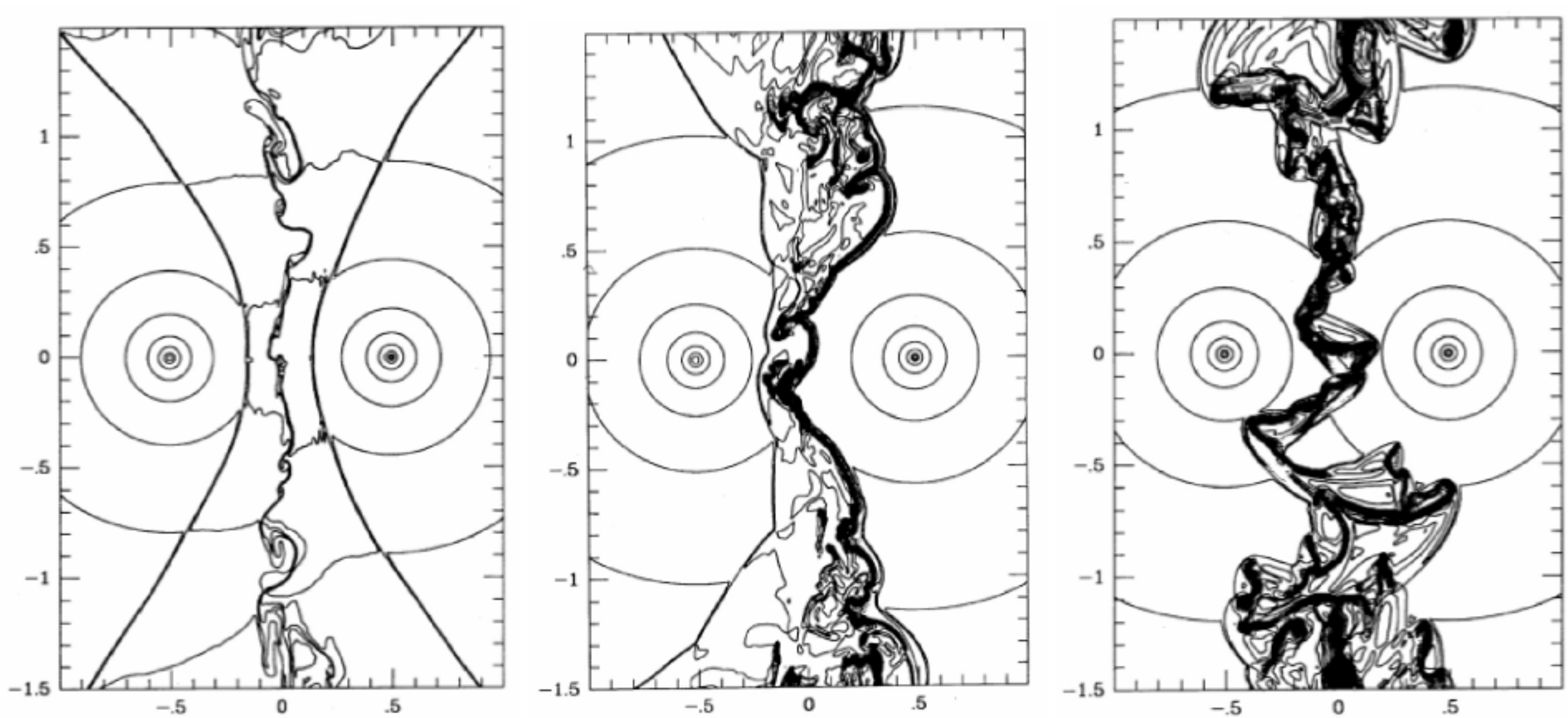

Figure 1: Instabilities in the WCR of CWBs. *Left:* When both sides of the contact discontinuity are largely adiabatic, the WCR is very smooth. *Center:* When one side is radiative, thin shell instabilities occur, but are somewhat limited by the "cushioning" of the hot gas (Vishniac 1983). *Right:* When both sides are radiative, the much stronger and highly non-linear thin shell instability occurs (Vishniac 1994). Adapted from Stevens et al. (1992).

SELF-REGULATED SHOCKS IN MASSIVE STAR BINARY SYSTEMS

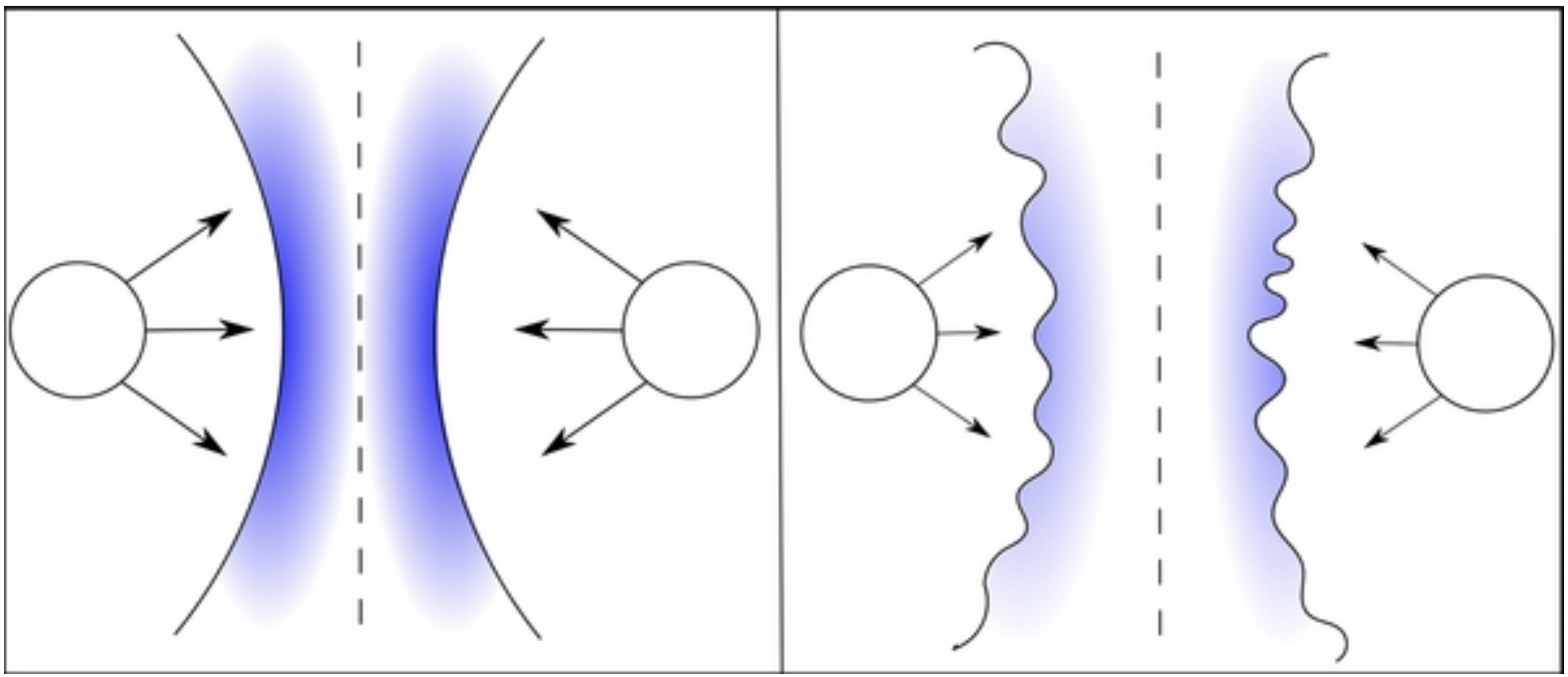

Parkin & Sim 2013 ApJ 767 114

SNR-stellar wind accelerator

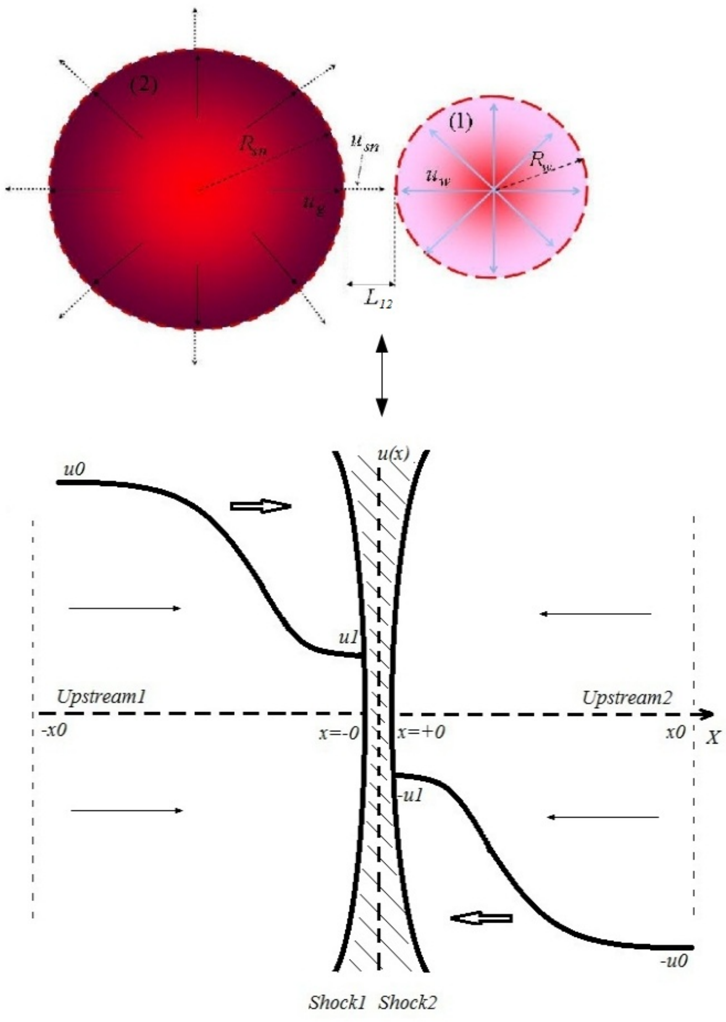

AB+ MNRAS V. 429, 2755, 2013

SNR-stellar wind accelerator
Non-linear kinetic model

Transport equation for CR distribution function

$$u(x)\frac{\partial f(x,p)}{\partial x} - \frac{\partial}{\partial x}\left[D(x,p)\frac{\partial}{\partial x}f(x,p)\right] =$$

$$= \frac{p}{3}\,\frac{du(x)}{dx}\,\frac{\partial f(x,p)}{\partial p} + Q(x,p)\delta(x). \qquad (1)$$

The momentum conservation equation, normalized to $\rho_0 u_0^2$ reads

$$U(x) + P_c(x) + P_w(x) + P_g(x) = 1 + \frac{1}{\gamma M_0^2}\,,$$

where M_0 is the Mach number of the unperturbed flow. The normalized cosmic ray pressure

$$P_c(x) = \frac{4\pi}{3\rho_0 u_0^2}\int_{p_{inj}}^{\infty} dp\; p^3\; v(p)\; f(x,p)\,, \qquad (2)$$

MNRAS V. 429, 2755, 2013

SNR-stellar wind accelerator

$$f(x,p) = f_0 \exp\left[-\int_x^0 dx' \frac{u(x')}{D(x',p)}\right]\left[1 - \frac{W(x,p)}{W_0(p)}\right], \quad (1)$$

$$\phi_{esc}(p) = -\frac{u_0 f_0}{W_0(p)} \quad (2)$$

where $D(x,p)$ is the CR diffusion coefficient,

cf Malkov' 97; Amato & Blasi 05; Caprioli + 11

$$W(x,p) = u_0 \int_x^0 dx' \frac{\exp\left[-\psi(x',p)\right]}{D(x',p)}, \quad (3)$$

$$\psi(x,p) = -\int_x^0 dx' \frac{u(x')}{D(x',p)}, \quad (4)$$

and $W_0(p) = W(x_0,p)$.

MNRAS v. 429, 2755, 2013

SNR-stellar wind accelerator II

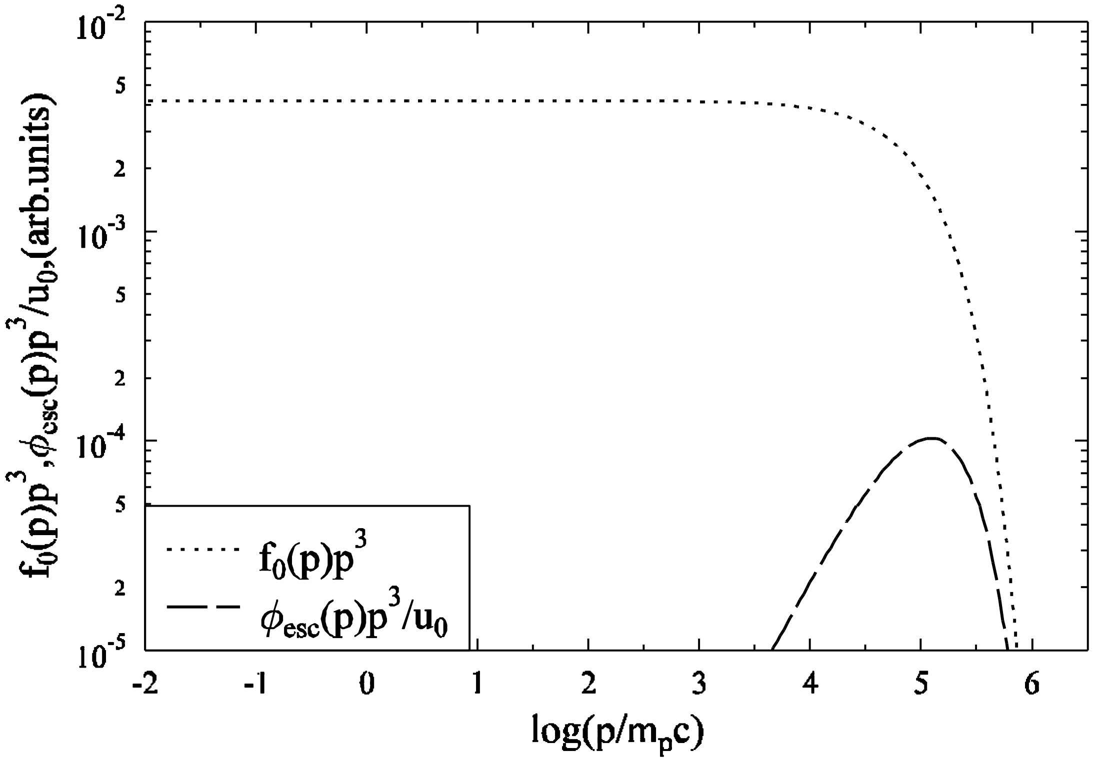

MNRAS V. 429, 2755, 2013

Energy Flux conservation

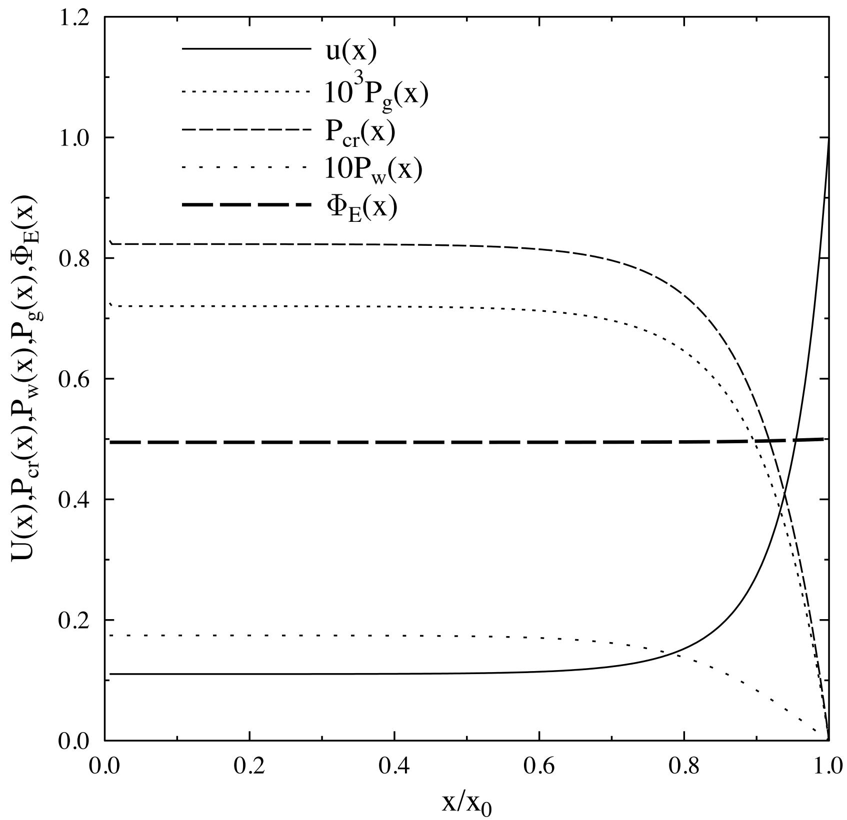

MNRAS V. 429, 2755, 2013

Particle acceleration between approaching shocks is one of the most efficient versions of Fermi I acceleration

Time dependent model

The telegraph equation to derive spectrum at Pmax

SNR-stellar wind accelerator

We solve one-dimensional transport equations for the pitch-angle-averaged phase space distribution function of protons, $f_p(x,p,t)$, and electrons, $f_e(x,p,t)$, given by

$$\tau(p)\frac{\partial^2 g_p}{\partial t^2} + \frac{\partial g_p}{\partial t} + u(x)\frac{\partial g_p}{\partial x} - \frac{1}{3}\frac{\partial u(x)}{\partial x}\left(\frac{\partial g_p}{\partial y} - 4g_p\right) = \frac{\partial}{\partial x}\left(D(x,p)\frac{\partial g_p}{\partial x}\right), \quad (1)$$

$$\tau(p)\frac{\partial^2 g_e}{\partial t^2} + \frac{\partial g_e}{\partial t} + u(x)\frac{\partial g_e}{\partial x} - \frac{1}{3}\frac{\partial u(x)}{\partial x}\left(\frac{\partial g_e}{\partial y} - 4g_e\right) = \frac{\partial}{\partial x}\left(D(x,p)\frac{\partial g_e}{\partial x}\right) + \exp(y)\frac{\partial}{\partial y}\left[b\exp(-2y)g_e\right], \quad (2)$$

where $g_p = p^4 f_p$, $g_e = p^4 f_e$, $y = ln(p)$.

MNRAS v. 429, 2755, 2013

SNR-stellar wind accelerator

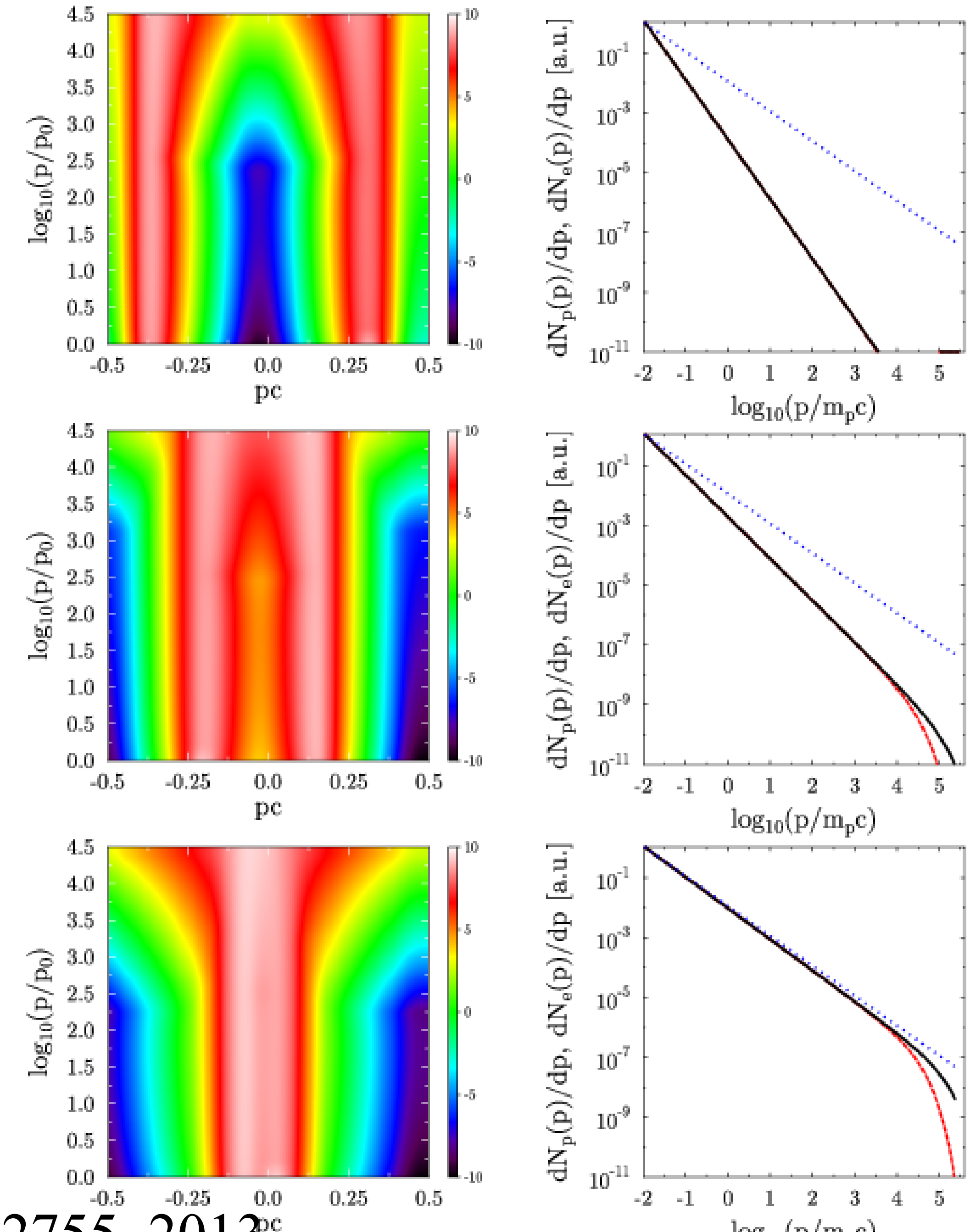

AB+ MNRAS v. 429, 2755, 2013

Temporal evolution of maximal energy of the accelerated CRs
Modest case of 3000 km/s SNR shock
Pevatron: shock is somewhat faster

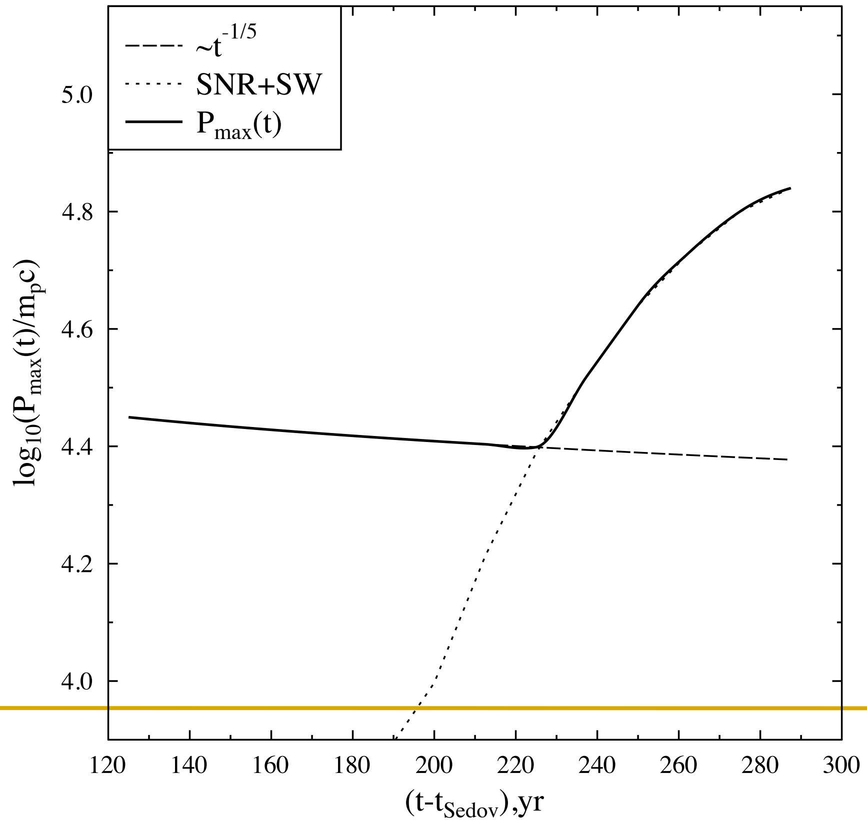

Supernova - wind “collision” system can provide Pevatron source in compact clusters

SNR-stellar wind non-thermal emission spectra I

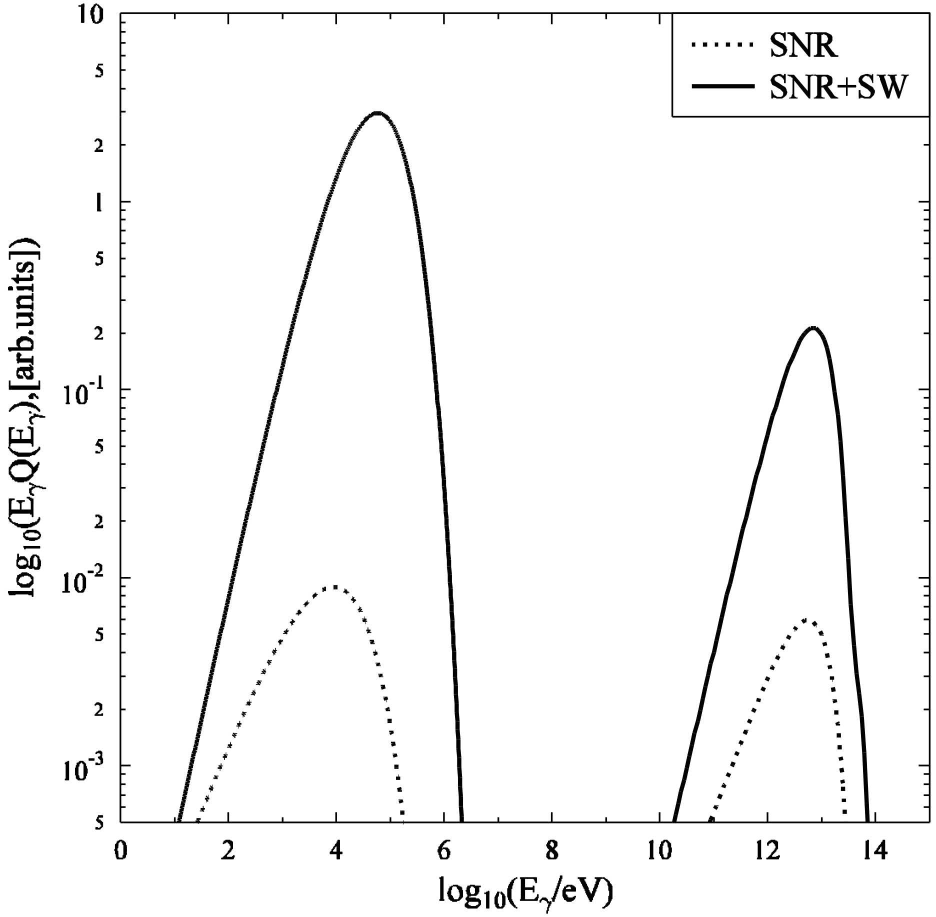

MNRAS v. 429, 2755, 2013

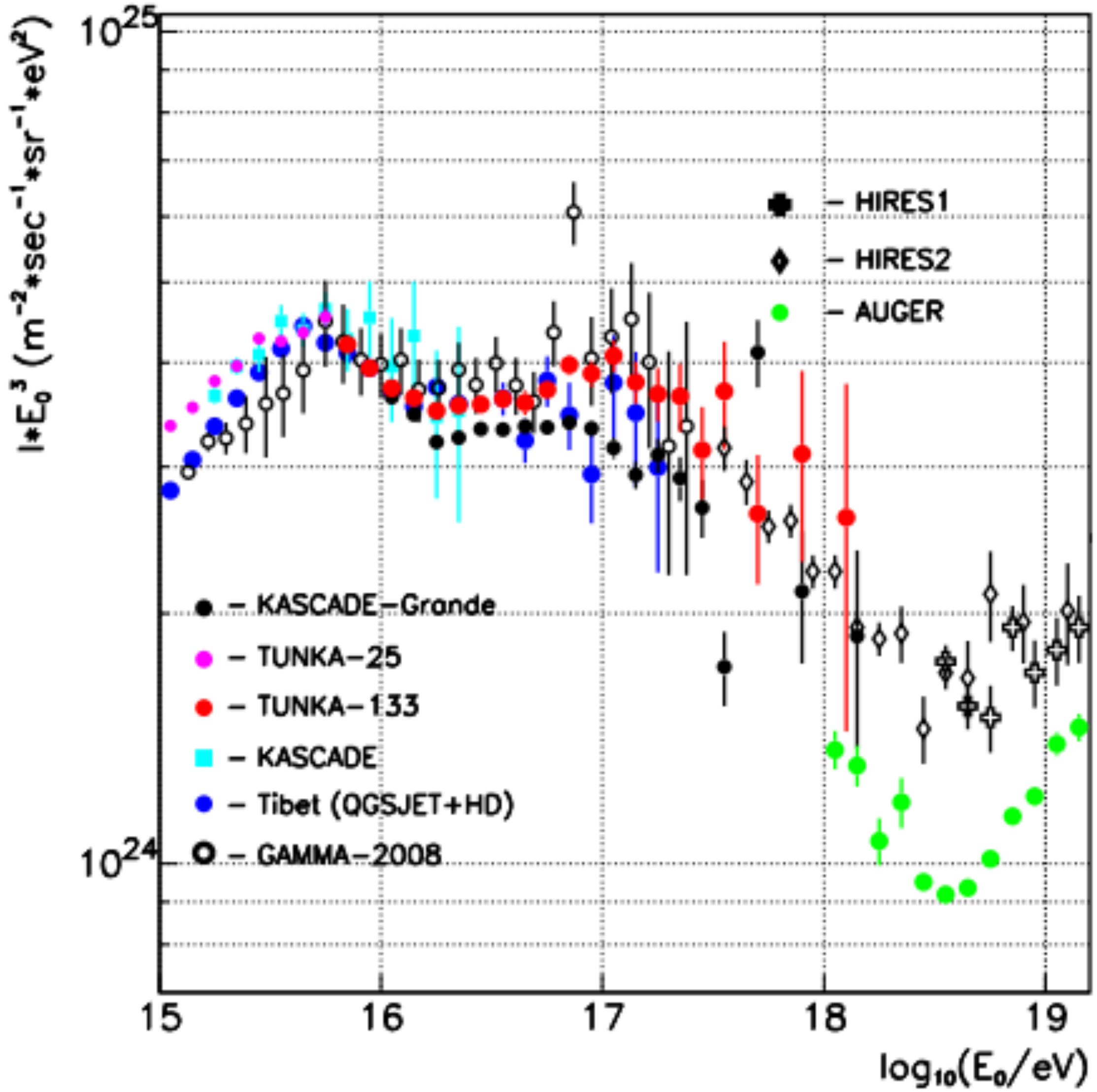

Figure 8: Tunka-133 all particle energy spectrum in comparison with results of other experiments.

Cosmic Ray Spectrum

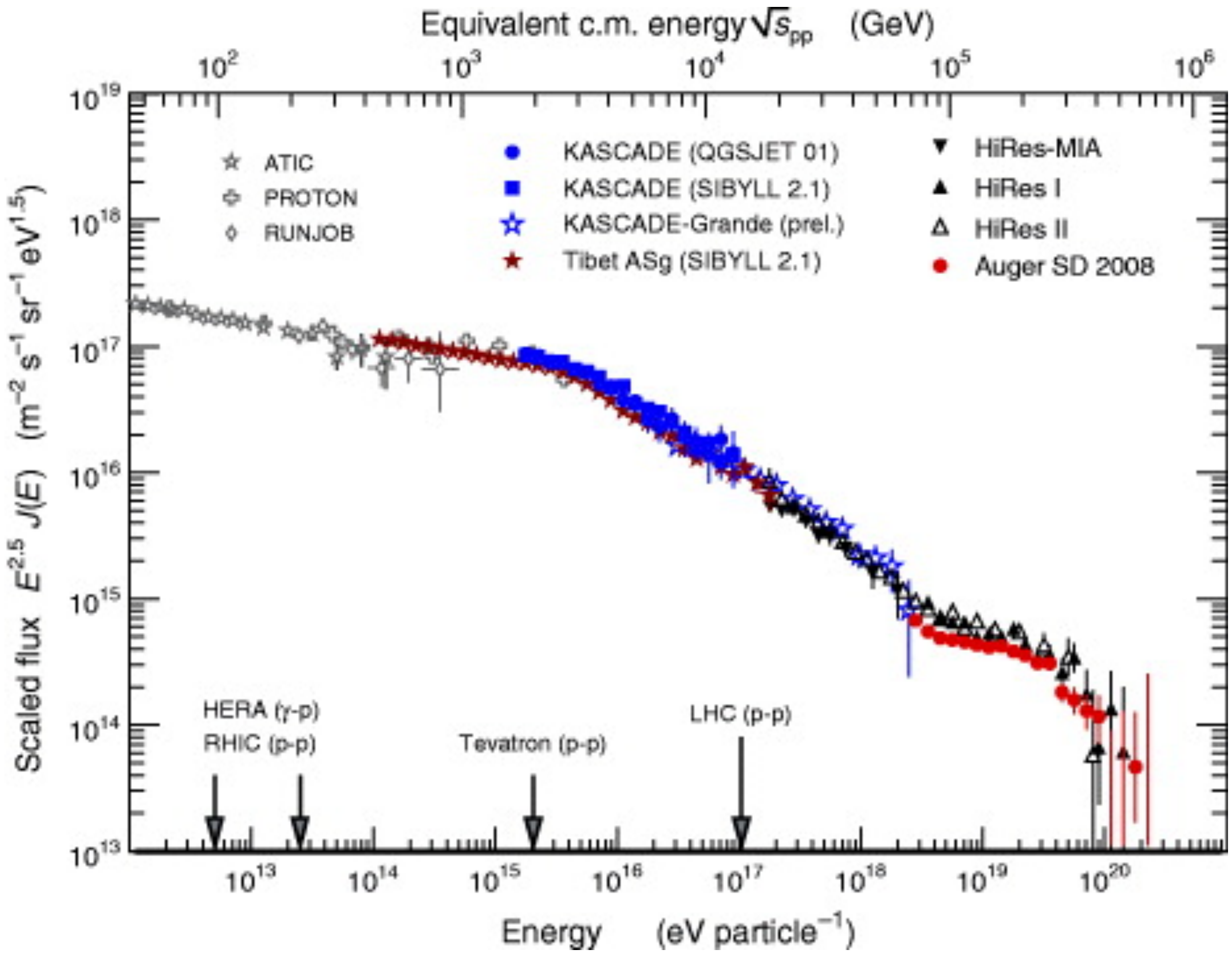

Blümer + 2010